https://doi.org/10.2352/ISSN.2470-1173.2019.13.COIMG-148

Fully-automatic Synthesizing Method of Dental Panoramic Radiograph by Using Internal Curve of Mandible in Dental Volumetric CT

Sanghun Lee, Seongyoun Woo, Chulhee Lee
School of Electrical and Electronic Engineering
Yonsei University
Seoul, South Korea
chulhee@yonsei.ac.kr

Joonwoo Lee, Jaejun Seo
IT R&D Center
Dio Implant
Seoul, South Korea
billlee@dio.co.kr, sjj@dio.co.kr

***Abstract*—Compared to conventional dental panoramic radiograph, synthesizing panoramic radiograph directly computed from dental cone-beam computed tomography (CBCT) images provides high-resolution images with reduced geometric distortion. Previous approaches required manual operations or were based on CBCT images without metal artifacts or missing teeth. In this paper, we introduced a fully-automatic method that can be applied to CBCT scans under severe conditions, which consist three main steps: bone and teeth segmentation, mandible curve extraction, and panoramic mapping. An adaptive method was first used for bone and teeth segmentation. Then the internal mandible curve, which provides a stable curve regardless of metal artifacts or missing teeth, was extracted and utilized for panoramic mapping. Our synthesizing method showed stable performance on various CBCT data sets.**

Keywords—computed tomography, radiography, biomedical imaging

I. Introduction

As one of non-invasive dental diagnostic methods, panoramic radiograph has played an important role in dental practice. In spite of its limitations in image quality, panoramic radiograph has been widely used as a supplement for diagnosis of dentistry diseases [1] because of its low radiation dose compared to medical CT and cone beam dental CT (CBCT) [2]. Also, panoramic radiograph provides preoperative dental information of mandibular and maxillary regions that can be used for human identification [3], planning of dental implants, etc. Modern dental CBCT systems also provide synthesized panoramic radiographs that are reconstructed from CBCT images. Unlike the conventional panoramic radiographs, synthesized panoramic radiographs are in relatively high resolution and have reduced geometric distortion [4], so they have gained more popularity.

Researchers have studied some methods of synthesizing dental panoramic radiograph from CBCT data sets. Tohnak *et al.* introduced a semi-automatic method that utilizes a handcrafted binary mask for the detection of dental arches [3]. Bing *et al.* used maximum intensity projection (MIP) to automatically find dental arches on mandibular CBCT data sets [4]. Recently, Luo *et al.* proposed a method to automatically synthesize dental panoramic radiographs from various types of dental CBCT data sets including closed-bite and open-bite shaped ones [5]. However these approaches were based on the data sets without artifacts or missing teeth. Thus under such severe conditions, those approaches based on teeth detection might fail. Especially, planning dental implants needs preoperative structural information of maxillofacial regions. Also, metal artifacts may occur when there are dental implants or dental fillings. Metal artifacts tends to appear heavily in the mandibular or maxilla teeth regions.

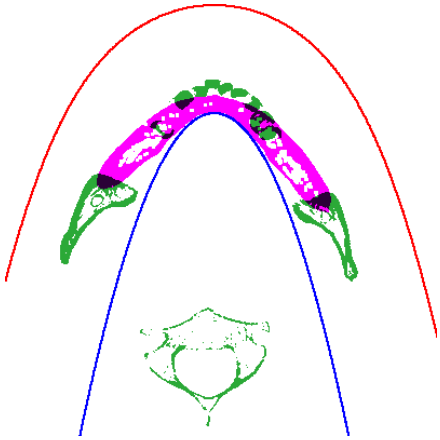

Fig. 1. Pink and green objects were automatically obtained from binarized CBCT slices that contained mandible and mandibular teeth. Blue and red lines represent the estimated internal curve of mandible and its equidistant curve with distance $U = 40mm$.

The mandible, a lower jawbone, is relatively dense and thick. It has curvatures similar to dental arches. Thus we propose to use the internal mandible curve to synthesize panoramic radiographs with CBCT data sets under severe conditions. Based on the internal mandible curve, we computed an equidistant curve for panoramic mapping (Fig. 1). The rest of the paper is organized as follows: methodology, an introduction of our data sets, and synthesizing results.

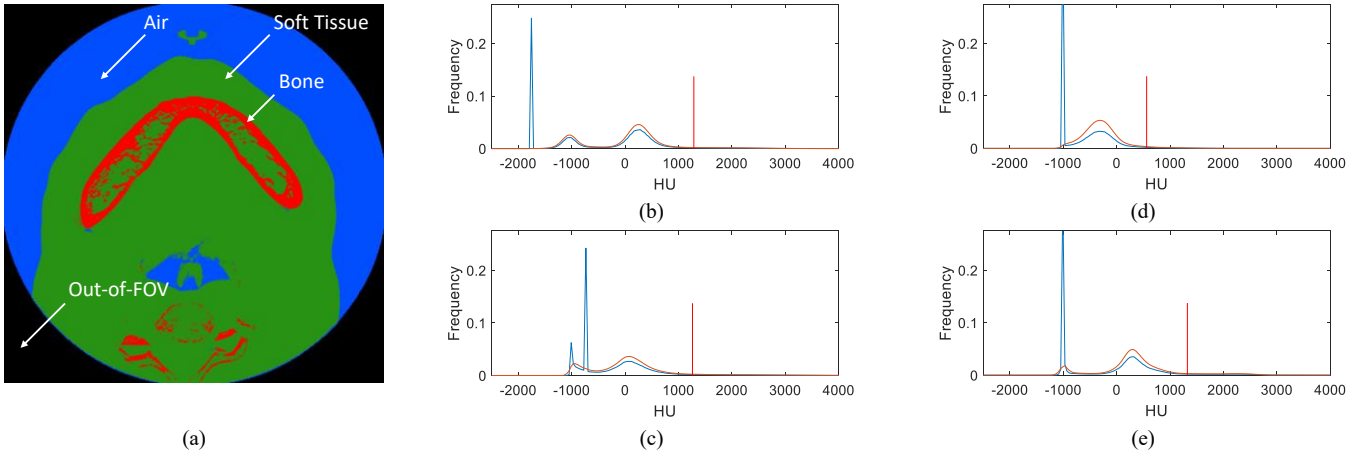

Fig. 2. (a) A false-color image of a slice of CBCT. Black, blue, green and red colored regions represent out-of-FOV, air, soft tissue and bone regions. There were four different types of histograms of CBCT: (b) Out-of-FOV voxels appeared as a spike outside of the air peak at around -1000 HU and the soft tissue peak at around 100 HU, (c) the spike appeared between two peaks, (d) two peaks were merged into a single peak, and (e) the out-of-FOV spike was merged with the air peak.

II. Methodology

Our work was based on the CBCT data sets that follow the Digital Imaging and Communications in Medicine (DICOM) standard. A CBCT data set was composed of two-dimensional CBCT slices with width W and height H that were in the DICOM file format. DICOM file header provided information on slice thickness d and pixel spacing (w and h) that define the physical size of a voxel. The proposed method for synthesizing panoramic radiograph from dental volumetric CT images consists three main steps: bone and teeth segmentation, extraction of the internal mandible curve, and panoramic mapping.

A. Bone and Teeth Segmentation

Discriminating bones and teeth from other objects including soft tissues or air regions is a prerequisite for obtaining the internal mandible curve. In medical CT scans, Hounsfield unit (HU) scale is widely used as a standard measure of radiodensity. Applying a conventional threshold method to HU is a simple way to find bones and teeth since HU values of medical CT are accurate and clinically reliable. However, bone density had a wide range of HU values due to the following reasons. First, the cortical bone usually had higher bone density values than cancellous bones. Also, the bone density varies depending on sex, age, etc. Thus, exact bone and teeth HU values may vary depending on patients. Moreover, compared to medical CT, HU values measured in CBCT scans may not translate to accurate radiodensity. Even for an object with the same radiodensity, gray levels may appear differently depending on their relative positions. Also, dental CBCT manufacturers have their own systems for interpreting raw gray values as HU. Consequently, although it had been reported that HU of medical CT and gray values of dental CBCT were highly correlated [7, 8], HU bone densities values provided by CBCT systems can be erroneous and unreliable [9].

To minimize the HU differences between CBCT data sets from different patients and various CBCT scan systems, we used a histogram-based approach to find appropriate a bone HU value adaptively for each CBCT scan. For our CBCT data sets, we used a 256-bin histogram of HU values. It was observed that CT histograms were classified into several categories by the location of peaks and spikes. In Fig. 2, blue curves shows four main categories of CT histograms: a spike outside of two peaks, a spike between two peaks, a spike at the tail of one peak, and a spike far from a peak. In our data sets,

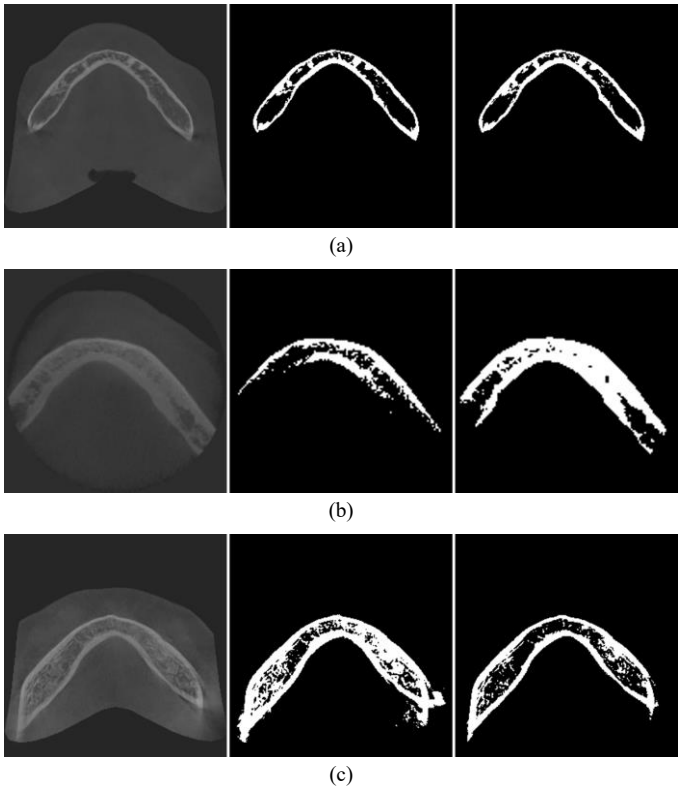

Fig. 3. Images in the left, center and right column are original images, binary images with a fixed bone HU value and output images of our adaptive method, respectively. (a) Well-segmented, (b) under-segmented and (c) over-segmented results with the fixed bone HU values whereas our method produced more stable outputs.

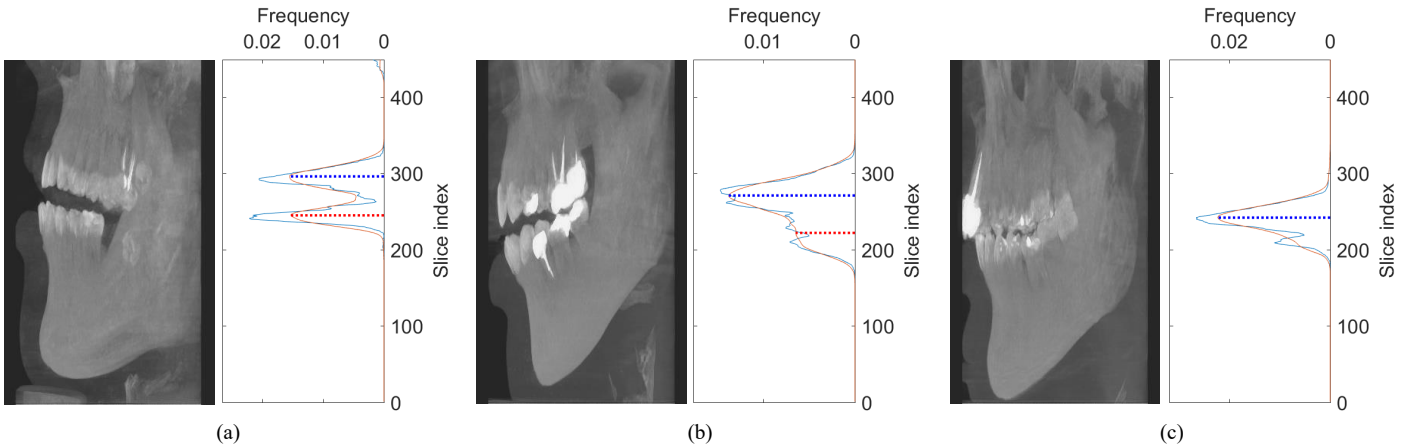

Fig. 4. Light blue and orange curves are normalized frequencies of enamel voxels and their moving averaged results with the 5 mm window. (a) CBCT data sets with the patient biting on bite block. Two peaks appeared clearly in both mandibular (red-dotted line) and maxilla (blue-dotted line) teeth regions. (b) The head orientation made two peaks almost merged into one peak. (c) When the bite block was not used, a single peak usually appeared.

histograms usually had two peaks and one spike as shown in Fig. 2(a). The two peaks near -1000 HU and 100 HU were associated with the air and soft tissue regions, respectively. Spikes appeared mainly because the voxels that lie outside of the field of view (FOV) had almost the same gray level. However, as can be seen in Fig. 2(b-c), HU values of out-of-FOV voxels were sometimes equal to or higher than that of air regions. In other words, spikes can appear anywhere on histograms. Moreover, there existed various types of FOV such as a circle-shaped FOV (Fig. 2(a-c)), a stitch of small FOVs [10] or an arch-shaped FOV (Fig. 2(d)). Especially, air region peaks were sometimes merged with spikes as shown in Fig. 2(c-d). To ignore the effects of out-of-FOV voxels on histograms, we directly suppressed those spikes by applying a moving median filter with a 5-bin window, since spikes usually occupied 1 or 2 bins. As shown in red curves in Fig. 2, we renormalized histograms after spikes were removed. Then the soft tissue HU value (x_s) was obtained by finding the center of the soft tissue peak. The soft tissue radiodensity value is usually at around 20-40 HU and that of bones is around 1000 HU [11]. So the bone HU value x_b was calculated as,

$$x_b = x_s + \alpha \tag{1}$$

where α is a constant that denotes the difference between the soft tissue and bone HU values. Although HU bone densities provided by CBCT systems may not be reliable, $\alpha = 900$ was applicable for most of our data sets. However, there were some data sets in low contrast that the HU differences between air and soft tissue regions were relatively small compared to other data sets. In this case, α should vary adaptively. Based on the definition of the Hounsfield scale, which was based on -1000 HU for air and 0 HU for water, we used the HU differences between the air and soft tissue regions for histogram normalization. Let σ_n be the mean of standard deviations of the histograms in normal conditions. We computed σ_n from our CBCT data sets of which HU difference between air and soft tissue regions was in normal ranges (1000-1100). Then we computed the standard deviation σ of each histogram, and calculated the bone HU value x_b as follows:

$$x_b = x_s + \alpha(\sigma_n / \sigma). \tag{2}$$

In other words, the difference between the soft tissue and bone HU values was adjusted based on the contrast of each data set. In this paper, we used $\sigma_n = 0.01$. Fig. 3 shows some examples when we used a fixed bone HU and adaptive bone HUs for image binarization. Images in the middle column of Fig. 3(a-c) show well segmented, under-segmented and over-segmented examples when a fixed bone HU $x_b = 1000$ was used, respectively. Applying our adaptive method on CBCT data sets showed stable performances.

B. Extraction of Internal curve of Mandible

Compared to dental arches, the internal mandible curve has a relatively stable shape even under harsh conditions such as metal artifacts, so we tried to utilize the curve for synthesizing panoramic radiograph. Bone and teeth segmentation results may contain cervical vertebrae, mandible, and maxilla. Thus the separation of mandible from other objects must be done first.

To find the mandible position in a CBCT volume, we used the mean physical distance between mandible and mandibular teeth. It is reported that the human permanent teeth length is approximately 22~28mm and the mean crown length is usually around 10 mm [12, 13]. Thus the mandible location can be estimated if we first locate the mandibular teeth in the direction of the axial axis. Teeth usually contain enamel, which is the visible part of the human tooth. Enamel has high HU values (above 2000 HU [14]) in dental CBCT since it is the hardest part of the human body. We binarized CBCT images with the enamel HU value ($x_e = x_s + \beta(\sigma_n / \sigma)$) to find the mandibular teeth where $\beta = 2100$, which is similar to (2). The light blue curves in Fig. 4(a-c) show some examples of the frequencies of enamel voxels, and the orange curves are their moving

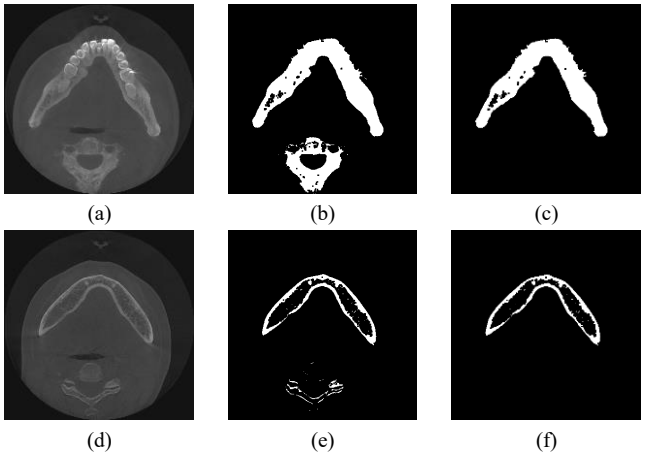

Fig. 5. (a) Maximum intensity projection of the mandibular part of CBCT. (b) Binarized and morphologically closed image of (a). (c) Biggest connected component of (b) remained. (d) An automatically selected slice that contains mandible. (e) Binarized and morphologically closed image of (d). (f) Only mandible part remained.

averaged curve with a 5 mm window for stable peak detection. Usually, patients were asked to bite on a bite block before taking CBCT scans. So mandibular and maxilla teeth were relatively well separated as in Figs. 4(a-b). In this case, two peaks usually appeared. When the bite block was not used, only one peak appeared as shown in Fig. 4(c). We used 9mm and 12mm as the mean physical distance between the mandible and the middle of mandibular teeth for two and one peak cases, respectively. Since the physical slice thickness is provided by DICOM headers, the physical distance can be converted as the slice index difference. Fig. 5(d) shows an automatically estimated CBCT slice of the mandible.

However, further separation of mandible was required since the CT slice may also contain unwanted objects such as a part of the cervical vertebrae. To extract only the mandible body, we used maximum intensity projection (MIP) of the mandibular part of CBCT (Fig. 5(a)). After applying binarization and morphological closing operation, we performed connected component (CC) analysis to obtain the biggest CC (Fig. 5(c)) of the binarized MIP. Then the CC analysis result can also be applied to the binarized CBCT slice of mandible (Fig. 5(e)). Fig. 5(f) shows the resulting CCs in Fig. 5(e) that satisfied the following condition: CCs intersected with the biggest CC at least 10% of their pixels.

C. Mapping

All the pixels at the bottom of each mandible CC were selected as the candidate pixels for the internal mandible curve. We first found a dominant pixel among the candidate pixels and retain only one-third of candidates around the dominant pixel. Quadratic polynomial curve fitting was then applied to these pixels to estimate the internal mandible curve. The obtained quadratic curve Q was represented as a parametric equation as follows:

$$\begin{aligned} x &= t \\ y &= at^2 + bt + c \end{aligned} \tag{3}$$

where $t \geq 0$. Then, an outer equidistant curve C_u with distance $u \geq 0$ from the curve Q was then represented as,

$$\begin{aligned} x' &= t + \frac{u}{s}\frac{dy}{dt} = t + \frac{u}{s}(2at + b) \\ y' &= at^2 + bt + c - \frac{u}{s}\frac{dx}{dt} = at^2 + bt + c - \frac{u}{s} \end{aligned} \tag{4}$$

where

$$s = \left[\left(\frac{dx}{dt}\right)^2 + \left(\frac{dy}{dt}\right)^2\right] = (2ax + b)^2 + 1. \tag{5}$$

Forward mapping based on the transform $T:(t,u) \rightarrow (x', y')$, however, can cause some distortion. It is because the distance between two points on the $x'y'$-coordinate that are corresponding to (t,u) and $(t+1,u)$ may vary for an arbitrary t.

To resolve this problem, we tried to find equidistant points $p_U(z) = (x'(z), y'(z))$ on the curve C_U where $z \in ¥$ and U is an empirically defined value. Their corresponding points on tu-coordinate are $(t_U(z), U)$. Let $t_i = i\tau$ with an arbitrarily small constant τ and $i \in □$ and the corresponding point of (t_i, U) on the $x'y'$-coordinate is defined as $p_{i,U} = (x'_{i,U}, y'_{i,U})$. Also, let $s_{i,U} = \sum_{n=0}^{i} r_{i,U}$ where $r_{i,U} = \left\| p_{i,U} - p_{i+1,U} \right\|$ is the Euclidean distance between two points $p_{i,U}$ and $p_{i+1,U}$. For any small τ that satisfies $0 < r_{i,U} < 1$ for all i, it is trivial that there exists N that satisfies both $z - 1 < s_{N,U} \leq z$ and $z \leq s_{N+1,U} < z + 1$ at the same time. Then the approximated equidistant points $p_U(z)$ on the curve C_U was obtained on the $x'y'$-coordinate by using linear interpolation as follows:

$$p_U(z) = p_N \frac{s_{N+1,U} - z}{s_{N+1,U} - s_{N,U}} + p_{N+1,U} \frac{z - s_{N,U}}{s_{N+1,U} - s_{N,U}}. \tag{6}$$

Consequently,

$$t_U(z) = \tau N \frac{s_{N+1,U} - z}{s_{N+1,U} - s_{N,U}} + \tau(N+1) \frac{z - s_{N,U}}{s_{N+1,U} - s_{N,U}}. \tag{7}$$

When U is fixed, (4) was rewritten as,

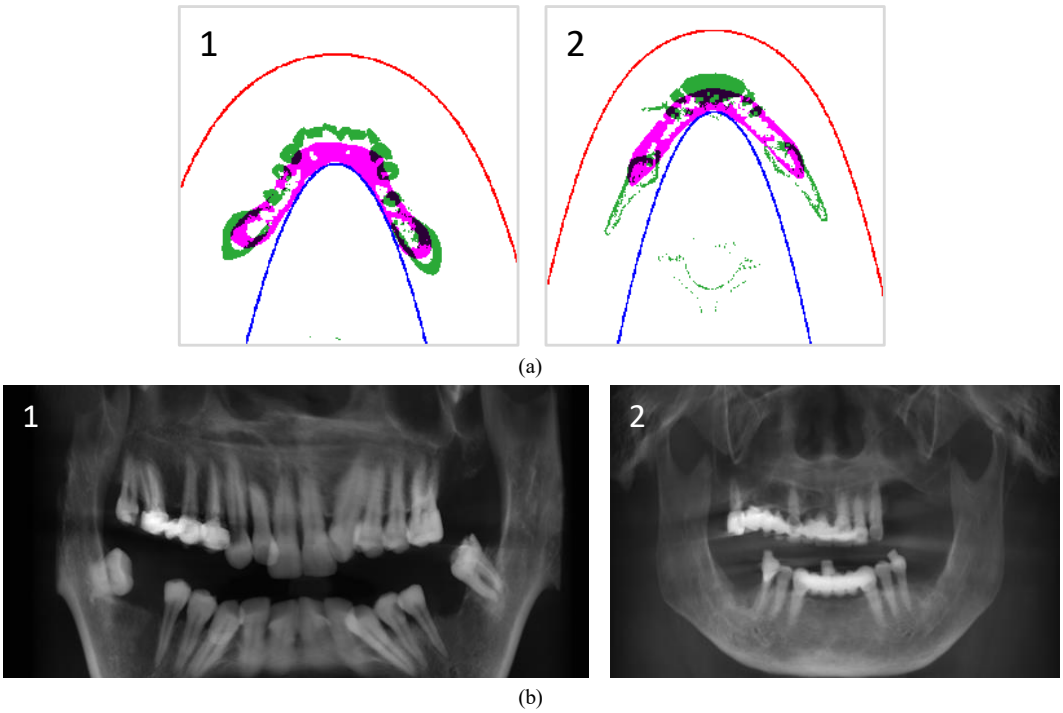

Fig. 6. (a) Blue and red lines are the obtained quadratic curves Q and the outer equidistant curve C_U with distance $U = 40mm$. The pink and green objects were automatically obtained from the binarized CBCT slices that contained mandible and mandibular teeth. (b) Corresponding synthesized panoramic radiograph.

$$x' = t_U(z) + \frac{u}{s}(2at_U(z) + b)$$
$$y' = at_U(z)^2 + bt_U(z) + c - \frac{u}{s} \quad (8)$$

Then, panoramic mapping was performed by the forward transform $T'_U : (z,u) \rightarrow (x', y')$. U should be large enough to cover the entire teeth. Also, the approximation will be more accurate when a smaller τ value is used. In this paper, we set $U = 40$ mm and $\tau = 0.1$. As a post-processing step, we the normalized image so that HU values $[-2500, 7500]$ to $[0,1]$ and applied a logistic function to all pixels to emphasize teeth voxels as follows:

$$y = 1/(1 + \exp(-20(x - x_b))) \quad (9)$$

where x and y are input and output intensity values, respectively. Finally, synthesized panoramic radiographs were obtained by averaging the panoramic mapping results in the direction of u-axis.

III. Data Sets and Results

The database comprises 102 CBCT data sets from different CBCT manufacturers. All CBCT data sets were in the DICOM format and rescale slope and rescale intercept values were provided by DICOM, which were used for calculating HU values from raw gray values. All voxels were rescaled to represent HU values before we applied the proposed method. Parameters used in this paper were empirically selected with five CBCT data sets and the others were not used.

Some results of the proposed synthesizing panoramic radiograph method are shown in Fig. 6. All the examples contained metal artifacts on teeth region. The CBCT data set of patient #1 (Fig. 6(b)) did not contain the entire region of mandible. Also, there were missing teeth for the patient #2 (Fig. 6(b)). As shown in Fig. 6(a), the internal curves of mandible and the outer equidistant curves were accurately obtained since the effect of metal artifacts were relatively small in the mandibular regions.

IV. Conclusions

In this paper, we proposed a synthesizing panoramic radiograph method that was based on the detection of the internal mandible curve. The curve had a similar shape with dental arch curves and could be obtained even under severe conditions such as metal artifacts or missing teeth. The proposed method comprises three main steps: bone and teeth segmentation, extraction of the internal mandible curve, and panoramic mapping. We proposed a stable method that adaptively finds bone HU values on CBCT data sets acquired from various CBCT systems. Also, a method for finding the mandible location in the direction of the axial axis on CBCT volume was also proposed. By using the internal mandible curve and its outer equidistant curve, we successfully synthesized dental panoramic radiograph on various CBCT data sets.

REFERENCES

[1] V. Rushton, and K. Horner, "The use of panoramic radiology in dental practice," *Journal of dentistry,* vol. 24, no. 3, pp. 185-201, 1996.

[2] T. Okano, and J. Sur, "Radiation dose and protection in dentistry," *Japanese Dental Science Review,* vol. 46, no. 2, pp. 112-121, 2010.

[3] S. Tohnak, A. Mehnert, M. Mahoney, and S. Crozier, "Synthesizing dental radiographs for human identification," *Journal of dental research,* vol. 86, no. 11, pp. 1057-1062, 2007.

[4] H. Bing, C. Liang, C. Zhen, P. Fang, L. Deyu, L. Shuyu, and F. Yubo, "An automatic method of synthesizing panoramic radiograph by unwrapping dental CT image," in Mechatronic Science, Electric Engineering and Computer (MEC), 2011 International Conference on, 2011, pp. 1094-1096.

[5] T. Luo, C. Shi, X. Zhao, Y. Zhao, and J. Xu, "Automatic synthesis of panoramic radiographs from dental cone beam computed tomography data," *PloS one,* vol. 11, no. 6, pp. e0156976, 2016.

[6] T. K. Papakosta, A. D. Savva, T. L. Economopoulos, G. K. Matsopoulos, and H. Gröhndal, "An automatic panoramic image reconstruction scheme from dental computed tomography images," *Dentomaxillofacial Radiology,* vol. 46, no. 4, pp. 20160225, 2017.

[7] M. Cassetta, L. V. Stefanelli, A. Pacifici, L. Pacifici, and E. Barbato, "How Accurate Is CBCT in Measuring Bone Density? A Comparative CBCT ‐ CT In Vitro Study," *Clinical Implant Dentistry and Related Research,* vol. 16, no. 4, pp. 471-478, 2014.

[8] T. Razi, M. Niknami, and F. A. Ghazani, "Relationship between Hounsfield unit in CT scan and gray scale in CBCT," *Journal of Dental Research, Dental Clinics, Dental Prospects,* vol. 8, no. 2, pp. 107, 2014.

[9] R. Pauwels, R. Jacobs, S. R. Singer, and M. Mupparapu, "CBCT-based bone quality assessment: are Hounsfield units applicable?," *Dentomaxillofacial Radiology,* vol. 44, no. 1, pp. 20140238, 2014.

[10] R. Pauwels, K. Araki, J. Siewerdsen, and S. S. Thongvigitmanee, "Technical aspects of dental CBCT: state of the art," *Dentomaxillofacial Radiology,* vol. 44, no. 1, pp. 20140224, 2014.

[11] G. N. Hounsfield, "Computed medical imaging," *Medical Physics,* vol. 7, no. 4, pp. 283-290, 1980.

[12] S.-Y. Kim, S.-H. Lim, S.-N. Gang, and H.-J. Kim, "Crown and root lengths of incisors, canines, and premolars measured by cone-beam computed tomography in patients with malocclusions," *The Korean Journal of Orthodontics,* vol. 43, no. 6, pp. 271-278, 2013.

[13] J. Verhoeven, J. Van Aken, and G. Van der Weerdt, "The length of teeth: A statistical analysis of the differences in length of human teeth for radiologic purposes," *Oral Surgery, Oral Medicine, Oral Pathology,* vol. 47, no. 2, pp. 193-199, 1979.

[14] M. Martorelli, P. Ausiello, and R. Morrone, "A new method to assess the accuracy of a Cone Beam Computed Tomography scanner by using a non-contact reverse engineering technique," *Journal of dentistry,* vol. 42, no. 4, pp. 460-465, 2014.

JOIN US AT THE NEXT EI!

IS&T International Symposium on

Electronic Imaging

SCIENCE AND TECHNOLOGY

Imaging across applications . . . Where industry and academia meet!

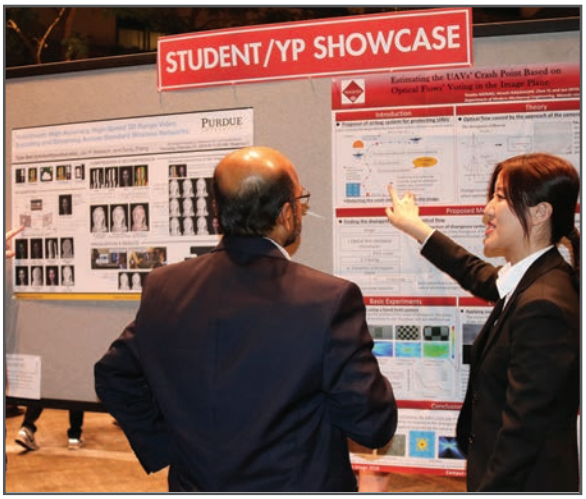

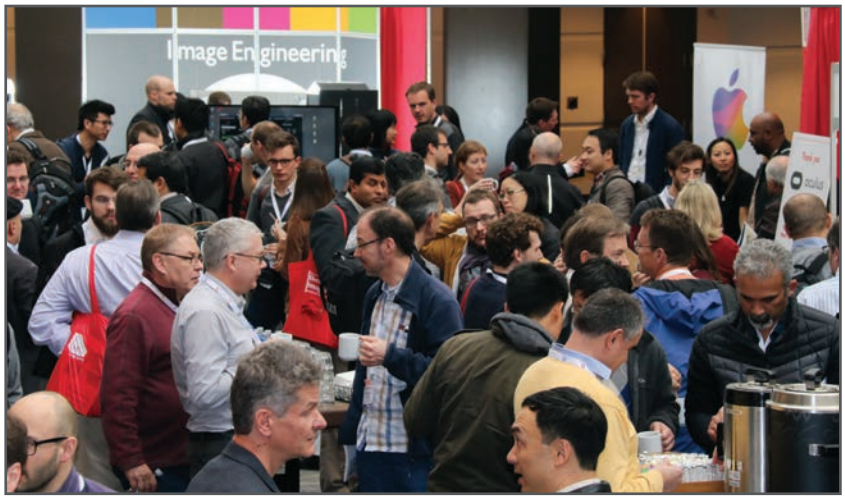

• SHORT COURSES • EXHIBITS • DEMONSTRATION SESSION • PLENARY TALKS •
• INTERACTIVE PAPER SESSION • SPECIAL EVENTS • TECHNICAL SESSIONS •

www.electronicimaging.org

IS&T
imaging.org